Chapter 8
Theoretical Aspects of Quantum Transport and Computational Modeling of Molecular Electronic Device

Hisao Nakamura

Abstract Recent techniques to create regulated nano-contact and precise measurement of transport properties such as current-voltage (IV) characteristics provide new insight of charge transfer and transport in a sub-10 nm-scale device. In this chapter, several theoretical concepts to bridge charge transfer (chemistry) and charge transport (physics) theories are described. "Old and new" problems of molecular electronics such as length and temperature dependence of conductance, unimolecular rectifier, etc. are revisited via a modern theoretical approach.

Keywords Quantum transport • Electron-phonon interactions • Molecular rectification • First-principles calculation • Nonequilibrium Green's function • Marcus theory

8.1 Introduction

Research of a molecular-scale device has been improved considerably by recent techniques to create regulated nano-contact [1–3] and precise measurement of transport properties such as current-voltage (IV) characteristics [4–9]. The pioneering work of molecular electronics is the proposal of a molecular rectifier by Aviram and Ratner (AR) [10]. Their idea was based on the analogue of a solid *pn* junction [11] to electron transfer between donor and acceptor molecules. However, several historical concepts of molecular electronics have been renewed [12–15], and, furthermore, potential advantages of molecular junctions have been discussed in broader research areas such as photovoltaic conversion [16–19], thermoelectricity [20–26], biosensor [27–29], memory [30–35], and so on. Hereafter, the terminology "molecular junction" represents a system consisting of a single molecule, molecular wire, or molecular film connected to metal electrodes. The varieties of functions relating to transport phenomena are mainly caused by a quantum confinement

H. Nakamura (✉)
Research Center for Computational Design of Advanced Functional Materials (CD-FMat), National Institute of Advanced Industrial Science and Technology (AIST), Tsukuba, Japan
e-mail: hs-nakamura@aist.go.jp

M. Kiguchi (ed.), *Single-Molecule Electronics*, DOI 10.1007/978-981-10-0724-8_8

effect to electrons passing through molecules [36–39]. A quantum confinement effect often gives a characteristic transport behavior by discrete resonant states, an interference effect, and so on. It depends on competition of the intrinsic molecular property (i.e., molecular orbitals: MO) and the contact effect of the molecular conductor and metal electrodes. In this sense, understanding quantum transport mechanism required fusion of the MO theory and Green's function theory or the scattering theory.

Green's function framework is very convenient to perform theoretical analysis for molecular junctions since correction terms, e.g., field effect, electron-electron interactions, and electron-phonon interactions, can be introduced systematically by self-energy terms. Nonequilibrium Green's function (NEGF) theory is often adopted for modeling transport processes under finite bias voltage [40–43]. In the past decade, the atomistic computational modeling of molecular junctions has been rapidly developed by combination of NEGF and first-principles mean-field theory, in particular density functional theory (DFT) [44–54]. The NEGF-DFT approach becomes now a standard tool since DFT has better computational scalability to the system size than other electronic structure theories. However, there are some limitations in first-principles approach yet. For an example, behavior of conductance and transport mechanism depend on length scale of molecular wire or thickness of the film. It is difficult to analyze these universal behaviors by only first-principles calculations due to huge computational demands. Therefore, theoretical modeling and computational study based on first-principles calculations should be adopted complementarily to understand fundamental mechanisms and design a new functional device.

In this chapter, the aim is to sketch theoretical aspects to understand the quantum transport process in molecular junctions based on concerto of theoretical and computational models with reference to recent experimental studies. Throughout this chapter, the atomic unit ($e = \hbar = 1$) is adopted to present theoretical formulations as far as there is no declining.

8.2 Theory of Electric Transport in Molecular Junctions

In order to realize a functional molecular device, the first step is to understand charge migration mechanism and control it. Theoretically, two opposite mechanisms are usually considered. One is coherent transport, which consists of a tunneling (band-like) transport, and the other is hopping mechanism as decoherence limit of charge migration [55, 56]. The former mechanism is dominant when length scale of the conductor is shorter than the mean free path length of the charge carrier (electron/hole). On the contrary, the latter mechanism assumes that the carrier loses its coherence by electron-phonon interaction, i.e., quantum nature of a carrier is lost in the hopping mechanism. In practical molecular junctions, the two mechanisms *coexist*. Coherence can survive locally over several molecular units though the charge migration is sequential hopping between each moiety of unit groups. Hence,

the suitable definition of "hopping site" depends on intrinsic electric structures of molecular units when one applies hopping model to a practical system. However, the two mechanisms show distinct universal length [57–60] and temperature [61, 62] dependence of electric conductance. Crossover of the universal behavior of conductance is expected as its dependence on the molecular wire length (L) and temperature (T) when the conductance measurement is examined by varying L and T in a wide range.

It is well known that the conductance decreases exponentially as a function of L, $\sigma = \sigma_0 \exp(-\beta L)$ [55, 63], for conjugated organic molecular wires when L is sufficiently short. The constant σ_0 is determined by the structure of the contact. The exponential behavior was measured for many conjugated molecular wires, and the β value is $10^{-1} \sim 10^{0}$ Å^{-1} for most conjugated molecules [64–67]. Observation of "length dependence crossover" has been also reported by several groups, and the crossover is usually explained by change of the coherent to hopping mechanism [57, 64, 68–70]. Choi and coworkers made oligophenyleneimine (OPI) wires bounded to Au substrates [64]. They found length dependence crossover at $L \sim 4.0$Å. The fitted β is 0.30 Å^{-1} in short L, while it is 0.09 Å^{-1} for $L > 4.0$ Å. Length dependence was measured systematically for similar oligomers, i.e., oligophenylenetriazole (OPT) [57] and oligonaphthalenefluoreneimine (ONI) [68] wires by Frisbie's group. In all cases, clear crossover is presented at the length of four or five molecular units, and they claim that the plot behaves as linear function of L, i.e., "transition" of the mechanism from tunneling to hopping.

As shown later, exponential behavior of conductance σ is the typical feature of the off-resonant tunneling system, where the energy gap of the Fermi level (E_F) and conduction band of the molecular conductor is sufficiently large. On the contrary, β can be considerably small and σ becomes nearly constant as a function of L when tunneling is resonant, e.g., nanowire of metallic atoms. Instead of length dependence crossover, another characteristic behavior of σ is observed for monoatomic metal wires such as Au, Pt, and Ir atoms [71, 72]. Smit et al. observed an oscillatory evaluation of σ depending on the number of atoms in the chain being even/odd parity [71]. They concluded that the parity oscillation was universal for metal monoatomic chain and thus length dependence of σ is not always linear or exponential. These experimental findings suggest difficulty to identify the dominant transport mechanism only by analyzing β obtained by a limited number of wire length samples, and *simultaneous* consideration of L and T dependence is necessary. Below, the general theory and qualitative analysis of the universal behaviors are presented by using Green's function framework. An inelastic transport process by electron-vibron interaction is also treated as the extension of the same Green's function approach.

8.2.1 Length Dependence of Conductance and Charge Migration Mechanisms

In order to describe an analytical theory, the single-level tight-binding model is very useful. Here, the theoretical model and analysis by Asai and Fukuyama [73] is introduced, which consists of a uniform chain and cubic lattice electrodes. The schematic figure and symbols of tight-binding parameters are given in Fig. 8.1. The resulting model Hamiltonian is written as follows [73]:

$$H = H_L + H_R + H_{\text{wire}} + H_T$$

$$H_{L/R} = \sum_{0<i_z} \sum_{k_x,k_y} \left(\varepsilon_{L/R} - 2t_M^{L/R} \left(\cos k_x a_{L/R} + \cos k_y a_{L/R} \right) \right) c^\dagger_{k_x,k_y,i_z} c_{k_x,k_y,i_z}$$
$$-t_M^{L/R} \sum_{i_z} \sum_{j_z=i_z\pm 1} \sum_{k_x,k_y} c^\dagger_{k_x,k_y,i_z} c_{k_x,k_y,j_z}$$

$$H_{\text{wire}} = \sum_{i=1}^{N} \varepsilon c_i^\dagger c_i - t \sum_i \sum_{j=i\pm 1} c_i^\dagger c_j$$

$$H_T = -t_L \left(c^\dagger_{I_1} c_1 + c_1^\dagger c_{I_1} \right) - t_R \left(c^\dagger_{I_N} c_N + c_N^\dagger c_{I_N} \right) \tag{8.1}$$

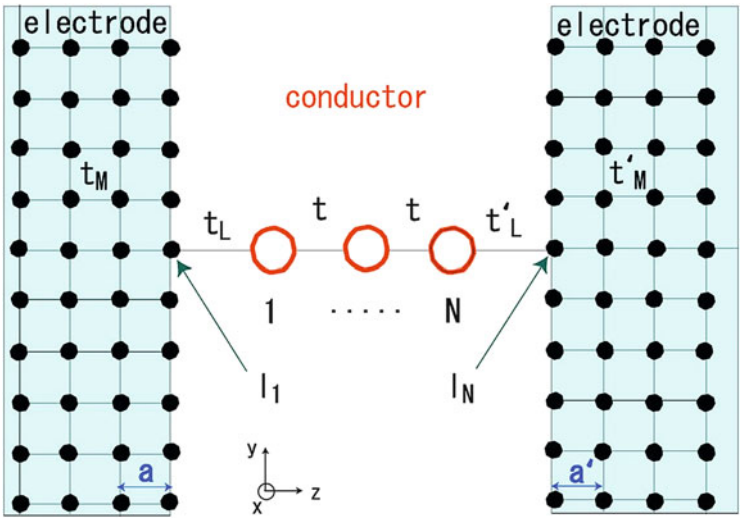

Fig. 8.1 A schematic view of the tight-binding model for the nano-contact composed of a monoatomic wire and electrodes [73]

The annihilation operator, $c_{kx,ky,jz}$, relates to an electronic state of the electrode labeled by two-dimensional band κ point (k_x, k_y) and real-space z (layer i_z). The operators c_i, c_{I_1}, and c_{I_N} are defined by the site in the chain and the left/right contact sites I_1/I_N, respectively. For simplicity, we take symmetric electrodes, i.e., the parameters are set as $t_M^L = t_M^R \equiv t_M, t_L = t_R \equiv t_c, \varepsilon_L = \varepsilon_R$. The cubic lattice constant is taken as $a_L = a_R \equiv a$. We set the metallic site energy of electrodes to zero. Hence, E_F is also zero when the metal is half-filling. Spin dependence of Hamiltonian is omitted in the present model.

Assuming that left and right electrodes are in thermal equilibrium, i.e., electrons are in Fermi distribution f, the electric current is expressed by NEGF formalism as follows [40, 43]:

$$I(V) = g_0 \int dE \mathrm{Tr}\left[\Gamma_L(E) G^r(E) \Gamma_R(E) G^a(E)\right] \left(f_L\left(E, \mu_L, T\right) - f_R\left(E, \mu_R, T\right)\right) \quad (8.2)$$

where V is bias voltage and equal to the difference of chemical potential of left and right electrodes and $\mu_L - \mu_R$. $G^{r/a}$ is retarded/advanced Green's function defined in the focused device region, which is usually termed as scattering region. $\Gamma_{L/R}$ is defined as $i\left(\Sigma_{L/R}^r - \Sigma_{L/R}^a\right)$, and $\Sigma_{L/R}^{r/a}$ is the retarded/advanced self-energy term of (semi-infinite) the left/right electrode. Trace part is transmission coefficient $\tau(E)$, and g_0 is conductance unit including spin factor. The conductance at zero bias and temperature T is obtained by

$$\sigma\left(T\right) = g_0 \int dE \tau(E) \left(-\frac{\partial f}{\partial E}\right) \quad (8.3)$$

When T is not sufficiently high, the derivative of the Fermi function in Eq. 8.3 is close to the delta function. Thus, conductance relates to the transmission coefficient at E_F. i.e., $\sigma(T) \approx \sigma \equiv g_0(E_F)$.

In the tight-binding model Hamiltonian, Eq. 8.1, Green's function and self-energy terms can be represented by an analytical form. The scattering region is the chain and the self-energy terms are added to the left/right terminal atomic sites of the chain. The resulting conductance σ is [73]

$$\sigma = 4\pi^2 g_0 t_c^4 \tilde{\rho}_c^2 \frac{\left|\lambda_1 - \lambda_2\right|^2}{\left|\left(\lambda_1 + \tilde{\Sigma}\right)^2 e^{i(N-1)\Theta_1} e^{\beta_1(N-1)} - \left(\lambda_2 + \tilde{\Sigma}\right)^2 e^{i(N-1)\Theta_2} e^{\beta_2(N-1)}\right|^2} \quad (8.4)$$

where $\lambda_{1/2} = \frac{\Delta}{2} \pm \sqrt{\frac{\Delta^2}{4} - t^2}$ and Δ is the energy gap $E_F - \varepsilon$. $\beta_{1/2}$ and $\Theta_{1/2}$ are defined as $e^{\beta_{1/2}} \equiv \left|\lambda_{1/2}/t\right|$ and $e^{i\Theta_{1/2}} \equiv \frac{\lambda_{1/2}/t}{\left|\lambda_{1/2}/t\right|}$, respectively. The retarded self-

energy of each electrode is

$$\tilde{\Sigma} = \pi t_L^2 \left[P \int \frac{dE'}{\pi} \frac{\rho_c (E')}{E' - E_F} + i\tilde{\rho}_c \right] \tag{8.5}$$

The term $\tilde{\rho}_c$ is the electron density of state (DOS) on the left (right) electrode terminal site I_1 (I_N) at $E = E_F$; $\tilde{\rho}_{l_{1(=N)}} E_F$ and $\tilde{\rho}_c$ are also calculated analytically. Equation 8.4 is useful to figure out the relation between conductance and the site energy level alignment, which is the most essential intrinsic parameter of molecular junctions. The analytical expression of β is derived straightforwardly from Eq. 8.4, and the parameter $\chi \equiv \left|\frac{\Delta}{2t}\right|$ gives threshold of the tunneling regimes. When $\chi > 1$, $\Theta_{1/2} \approx 0$ and $\beta_{1/2} \approx \ln\left(\left|\left|\Delta/2t\right| \pm \sqrt{\Delta^2/4t^2 - 1}\right|\right)$, respectively. When the tunneling is completely off-resonant, i.e., $y \gg 1$, the values of $\beta_{1/2}$ are $e^{\beta_1} \to \left|\Delta/t\right|$ and $e^{\beta_2} \to 0$. Hence, d_0, the conductance in the off-resonant tunneling, is expressed by the exponential function of L as

$$\sigma \approx 4\pi^2 g_0 t_c^4 \tilde{\rho}_c^2 \frac{\left|\lambda_1 - \lambda_2\right|^2}{\left|\lambda_1 + \tilde{\Sigma}\right|^2} e^{-\beta L} \tag{8.6}$$

where the distance between neighboring sites (molecular units) is set to d_0 and β is

$$\beta = \frac{2\ln(\Delta/t)}{d_0} \tag{8.7}$$

This analytical expression tells that there are distinct regimes of exponential and non-exponential behavior specified by a threshold value, i.e., $\beta_{th} = \frac{2\ln 2}{d_0}$.

On the contrary, $\chi \leq 1$, and the transport is resonant tunneling or band-like transport. One can find clear conductance oscillation as a function of L (or number of sites in the chain) by plotting Eq. 8.6 when the parameter is set to $\chi \leq 1$. When $\chi \approx 0$, the oscillation of σ is even/odd parity for the number of the sites in the wire. Furthermore, theoretical calculation predicts the change of parity (even/odd or odd/even) is reversible by change of χ. With increasing χ to 1, the periodicity of oscillation becomes large and infinite at $\chi \to 1$. Hence, validity of β estimated by a limited number of data by experiments or first-principles calculations has to be examined carefully when a system is more complex molecular wire (e.g., multilevel sites) and likely quasi-resonant tunneling, $\chi \approx 1$. Adding to length dependence, it is worthwhile to note the amplitude of conductance oscillation. The amplitude is governed by a ratio of transfer integrals, t_c^2/t_M and t. There is a threshold value, $\left|\frac{t_c^2/t_M}{t}\right|$, which gives perfect transmission, and the amplitude becomes large when deviation from the threshold increases.

Formulation of hopping mechanism is derived by the NEGF framework when the decoherence term such as electron-vibron interaction and electron-electron interaction is large. Here, the decoherence term is the coupling term of electron and

inter-/intramolecular vibration (vibron) in the present case though other terms (e.g., impurity scattering, electron-electron scattering) are also possible. It is sufficient to focus on only charge migration between the nearest neighboring sites of the wire. Following the argument by Yeganeh and coworkers [74], the simplified model Hamiltonian is adopted, where only the site "0" couples strongly with vibron (i.e., source of decoherence) of the wire:

$$H_{\text{wire}} = \varepsilon c_0^\dagger c_0 + \sum_i \varepsilon c_i^\dagger c_i - t\sum_i \sum_{j=i\pm1} c_i^\dagger c_j + M\left(b+b^\dagger\right) c_0^\dagger c_0 + \Omega_0 b^\dagger b \tag{8.8}$$

where M is electron-vibron coupling strength and $b^\dagger(b)$ is the creation (annihilation) operator of vibron, whose frequency is Ω_0. In the strong coupling limit, applying canonical transformation (Lang-Firsov transformation) [75, 76] is convenient:

$$\begin{aligned}\overline{H}_{\text{wire}} &= \exp\left(\tfrac{M}{\Omega_0} c_0^\dagger c \left(b^\dagger - b\right)\right) H_{\text{wire}} \exp\left(-\tfrac{M}{\Omega_0} c_0^\dagger c \left(b^\dagger - b\right)\right) \\ &= \left(\varepsilon - \tfrac{M^2}{\Omega_0}\right)\bar{c}^\dagger \bar{c} - \bar{t}\sum_{i=\pm1}\left(\bar{c}^\dagger c_i + c_i^\dagger \bar{c}\right) + \varepsilon\sum_{i\neq0} c_i^\dagger c_i + t\sum_i\sum_{j=i\pm1}\left(c_i^\dagger c_j + c_j^\dagger c_i\right) \\ &= H_{\text{hop}} + \varepsilon\sum_{i\neq0,\pm1} c_i^\dagger c_i + t\sum_i\sum_{j=i\pm1}\left(c_i^\dagger c_j + c_j^\dagger c_i\right)\end{aligned} \tag{8.9}$$

The site "0" is the source of decoherence. The new operators, $\bar{c}$ and $\bar{t}$, are defined as $c_o \exp\left(\frac{-M}{\Omega_0}\left(b^\dagger - b\right)\right)$ and $t\exp\left(\frac{-M}{\Omega_0}\left(b^\dagger - b\right)\right)$, respectively. Focusing on the Hamiltonian of hopping site H_{hop}, charge migration rate is derived by using Eq. 8.2 where the left and right electrodes are replaced to the sites of $i \neq 0$ in Eq. 8.9. Then one gets the hopping conductance as $\sigma = -2\pi g_0 \bar{t}^2 \text{Im}G^r(\varepsilon)$. Green's function is now defined by H_{hop}. Since H_{hop} consists of the vibron term, we consider finite temperature Green's function, i.e.,

$$\begin{aligned}G^r(\varepsilon) = \sum_n \exp\left\{-\left(\frac{M}{\Omega_0}\right)^2 (2N_{BE}+1)\right\} I_n\left(2\left(\frac{M}{\Omega_0}\right)^2 \sqrt{N_{BE}\left(N_{BE}+1\right)}\right) \\ \times \exp\left(\frac{n\Omega_0}{2k_BT}\right)\left(\varepsilon - \left(\varepsilon_0 - \frac{M^2}{\Omega_0}\right) - n\Omega_0 + i\delta\right)^{-1}\end{aligned} \tag{8.10}$$

where I_n is the Bessel function. Introducing an asymptotic form of the Bessel function and after several algebras [74], the conductance is expressed as a high-temperature limit

$$\sigma \approx \frac{2\pi g_0 \bar{t}^2}{\sqrt{4\pi\lambda k_B T}} \exp\left[-\frac{\left(\tilde{\Delta} - \tilde{\lambda}\right)^2}{4\lambda k_B T}\right] \tag{8.11}$$

where $\tilde{\Delta}$ relates redox potential of the two sites and $\tilde{\lambda}$ is equal to $\frac{M^2}{\Omega_0}$. Equation 8.11 is formally similar with the electron transfer rate expression by the Marcus theory [55, 77]. The analogue of Marcus's electron transfer rate theory and charge migration by hopping mechanism (polaron) has been often adopted for analysis of organic semiconductor and polymer [78]. For many conjugated molecular wires, one hopping site can consist of two or more molecules and hopping is multi-step. Conductance is independent or linear to L when transport is dominated by hopping mechanism (decoherence limit). Equation 8.11 predicts Arrhenius-type thermal activation for hopping mechanism.

8.2.2 Universal Temperature Dependence Crossover and Inelastic Scattering Effect by Electron-Vibron Interaction

In Sect. 8.2.1, universal "length dependence crossover" and the two different charge migration mechanisms were described. Observation of sufficiently large thermal activation energy is considered to be a direct evidence of hopping mechanism. Equation 8.11 was proved by NEGF framework with strong coupling limit of electron-vibron interactions. However, it is not clear whether temperature dependence and relating thermal activation energy is decided uniquely or not by given L. As a theoretical view, a relating question arises: Is strong electron-vibron coupling a necessary condition to realize the Arrhenius-type behavior? The questions have been opened by Selzer et al. [61]. They used a sufficiently short molecule to avoid strong decoherence caused by large L: thus, transport is expected to be almost coherent. They observed temperature dependence crossover in the same 1-nitro-2,5-di(phenylethynyl-4-mercapto)benzene molecule. A similar crossover has been reported for biomolecular junctions, e.g., DNA molecule by Yoo et al. [79] and dry bacteriorhodopsin by Sepunaru et al. [80]. Recently, Lee et al. measured temperature dependence of a single oligothiophene molecular wire, where each measured wire contains 5 (5T), 14 (14T), and 17 (17T), respectively [81], as shown in Fig. 8.2. Temperature dependence crossover is not found in the short (5T) and long (17T) wires, and each conductance plot can be explained by coherence and hopping mechanisms as usual. However, in the middle length (14T), the conductance is almost unchanged $\left(\sigma \approx 1.8 \times 10^{-5} G_0\right)$ up to 350 K, and then it increases with increasing temperature $\left(\sigma \approx 1.8 \times 10^{-5} G_0\right)$ at $T = 450$ K. Since the length is fixed, strength of electron-vibron coupling should be the same. Hence, temperature dependence of decoherence term is responsible rather than dependence of coupling strength.

The same model Hamiltonian of Eq. 8.1 was applied, while electron-vibron interaction by the extended Su-Schrieffer-Heeger (SSH) model was added [81]. Contrary to the canonical transformation, the self-consistent Born approximation (SCBA) was adopted to calculate Green's function, i.e., strength of each coupling is

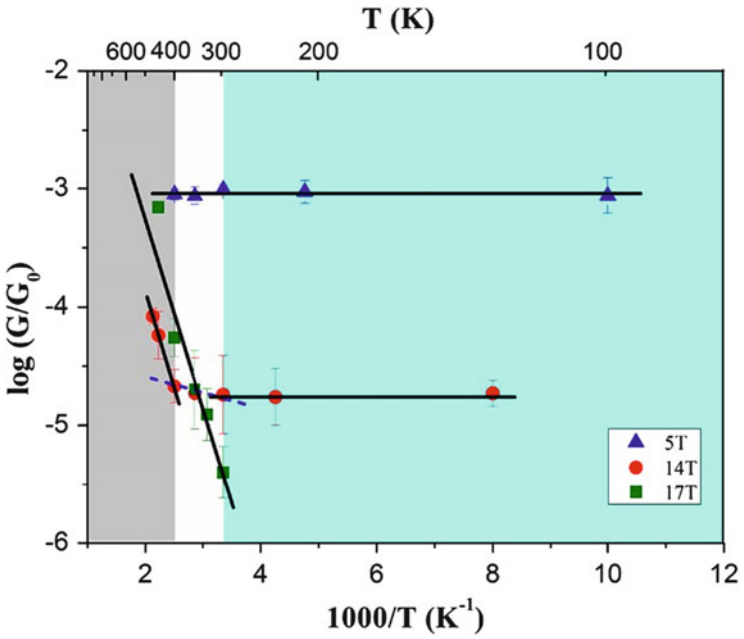

Fig. 8.2 Plots of temperature dependence of conductance for 5T, 14T, and 17T molecular junctions [81]

assumed to be sufficiently weak. In the SCBA, both nonequilibrium electron and vibron Green's functions (labeled as D) are determined simultaneously through electron-vibron self-energy terms, $\sum_{evib}$ (electron) and $\prod_{evib}$ (vibron) [82]. Interestingly, SCBA results in successes to reproduce a universal behavior of conductance σ in both low- and high-temperature regimes, i.e., nearly zero and large thermal activation energies. The temperature dependence of the SCBA results was nicely represented by the scaling function $S(T) = A\exp(-\tanh(B/T)) + C$, where the form of the function is derived by the single-mode polaron model. The parameter B represents the activation energy and corresponds to the lowest vibron energy. C is constant to match the conductance at a low-temperature limit and A is the adjust parameter. Scaling analysis by $S(T)$ to the experimental conductance was also applied and showed fairly well agreements with each other. Recall that the present Arrhenius-type behavior is obtained by SCBA of weak electron-vibration coupling approximation. Thus, Arrhenius-type σ and large activation energy are not evidence of the hopping mechanism of strong electron-vibron coupling. High temperature enhances decoherence and provides the thermal activation energy though strength of coupling is weak. In this sense, the concept of "hopping" mechanism should be extended.

As stated above, the electron-vibron interaction affects σ even when the interaction is weak. Only an inelastic process exchanges energy between electron and

vibron, while both of elastic and inelastic scatterings change electric current by resonance of electron and vibron. Rapid change of electric current is observed when the applied bias matches to the energy Ω_α of vibrational mode α. Hence, the plot of the second derivative of electric current by bias, $\frac{d^2I}{dV^2}$, provides a peak or dip at $V \approx \Omega_\alpha$ and is called inelastic electron tunneling spectroscopy (IETS) [83–90]. IETS is a fingerprint of the bridge molecule and useful spectroscopic tool to prescribe the bridge molecular species and adsorbed molecular conformation [91]. One of interest is that its shape (peak/dip) of IETS depends on a molecular wire [92]. The peak shape was usually observed in organic molecular junctions [87, 93–98], and the early theory of IETS showed that energy exchange of inelastic processes opens a new channel of tunneling electron, i.e., IETS gives a peak shape for positive bias (and dip for negative bias). On the contrary, Agrait et al. measured IETS of some metal atomic nanowires and found that the shape of IETS is dip at positive bias $V>0$ [99, 100]. As shown below, peak/dip relates roughly to that tunneling is off-resonant/resonant.

To analyze IETS, use of the normal mode coordinates is convenient to define vibron Green's function. Nonequilibrium effect and details of thermal dissipation of excited vibron energy is often omitted in IETS analysis. Within the model of a single site and single vibrational mode in the wire part like Eq. 8.8, the difference of I with and without electron-vibron interaction, δI, is evaluated simply by using the lowest-order Born expansion (LOE) [48, 101–103] with omitting the energy shift by the interaction. The second derivative of δI by bias is expressed as follows:

$$\frac{d^2(\delta I)}{dV^2} \approx g_0 M^2 \tau(E_F) \frac{\Delta^2 - (\Gamma_L + \Gamma_R)^2/4}{\left\{\Delta^2 + (\Gamma_L + \Gamma_R)^2/4\right\}^2} \frac{d^2F}{dV^2} \tag{8.14}$$

where the function F is only a function of V, T, and Ω_α:

$$F = (\Omega_\alpha - V) N_{BE}(\Omega_\alpha - V, T) - (\Omega_\alpha + V) N_{BE}(\Omega_\alpha + V, T), \tag{8.15}$$

and $N_{BE}(\omega, T)$ is the Bose-Einstein function. When Γ_L and Γ_R terms are almost equal, Eq. 8.14 leads to a more simple form as follows:

$$\frac{d^2(\delta I)}{dV^2} \to g_0 M^2 \tau(E_F)(1 - 2\tau(E_F)) \frac{d^2F}{dV^2}. \tag{8.16}$$

Equation 8.16 predicts clear peak/dip change at $\tau(E_F) = 0.5$, i.e., the sign of IETS depends on that tunneling is resonant (band-like) or off-resonant [104]. More detailed analyses have been performed by SCBA with changing the parameter $\triangle$ and t_M [105]. The resulting phase diagram gives the phase boundary of peak and dip as well. The boundary and that calculated by the condition $\tau(E_F) = 0.5$ agree qualitatively when the correction by real part of self-energies is considered. However, the agreement of SCBA and LOE is not sufficient when the values of $\triangle$

and t_M are small, which represents resonant tunneling at weak-link contact. In this region, multiple scattering effects will become important for IETS analysis.

8.2.3 MO Engineering and Contact Chemistry via First-Principles Calculations

Up to now, universal behavior of transport phenomenon of molecular junctions is discussed, and the simple model Hamiltonian approach was very useful for analysis. However, parameterization is very complicated for complex molecules or nanostructured wires, where quantum interference [36, 37, 106–108] due to topology, multi-site effect at an anchoring point, and multilevel effects play essential roles to device functions. Thanks to recent development of computational methods, in particular combination of NEGF and DFT [44, 47–51, 54, 109–112], first-principles transport calculation is possible. Once first-principles results are obtained, we can estimate observables like *IV* characteristic and extract convenient quantities to understand molecular-oriented device feature by using first-principles Green's functions, projected wave functions, and so on.

In the first-principles approach, the scattering region is defined as the region consisting of the molecular part and a sufficiently large number of atomic layers of left and right leads since the electronic structure of the contact (interface) region and deep bulk electrodes must be treated on the equal footings. The self-energy terms are added on the most outer region of the scattering region, i.e., deep bulk region. In NEGF-DFT, Kohn-Sham Hamiltonian is used to define Green's functions: thus, self-energy of electron-electron interaction is incorporated as mean-field potential, Hartree (V_H) and exchange-correlation (V_{XC}) terms. An external electric field due to bias voltage is also inserted to the Hamiltonian, and perfect screening is assumed in the electrodes. The mean-field approximation makes calculations easy since the relating lesser self-energy term is zero [43, 113]. The most time-consuming step is updating the density matrix and getting a converged result in self-consistent cycles since the numerical integral of the lesser Green's function by energy is necessary. Many algorithms and numerical techniques have been proposed to get fast SCF convergence and reduce computational cost [44, 48, 54, 114, 115]. There are several drawbacks in the standard NEGF-DFT, e.g., underestimating the HOMO-LUMO gap by omitting dynamical correlation, unknown V_{XC} function applicable to nonequilibrium condition, and so on. Several theoretical efforts have been reported such as an extension to time-dependent DFT framework [116–119], analysis of derivative discontinuity of XC functional [120, 121], and correction by partial GW approximation [122, 123]. In spite of these drawbacks, NEGF-DFT is still a useful and practical tool to perform first-principles transport calculations. Here, we introduce a few examples of the recent NEGF-DFT calculations to show the power of the first-principles transport calculation.

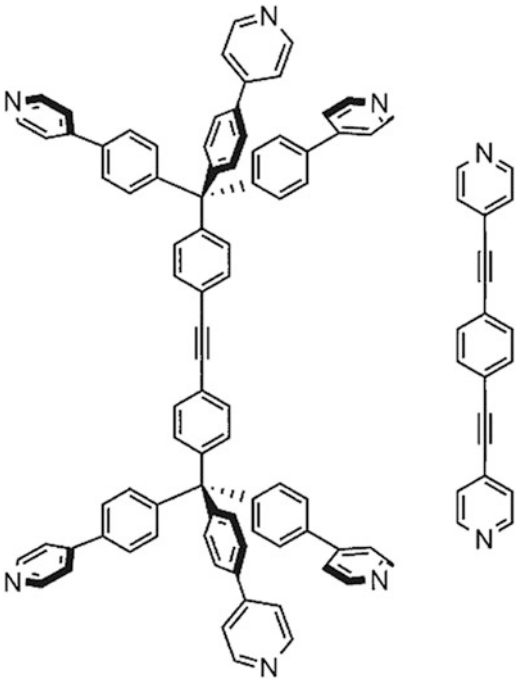

Fig. 8.3 Chemical structures of diphenylene-ethynylene with single (1Py) and tripodal-leg (3Py) anchors based on pyridine [124]

Designing robust anchoring is as important as synthesizing the conductor to avoid breaks of contact by heating or concentrated electric field. Recently, use of tripodal-leg anchor based on pyridine (**3Py**) was proposed as shown in Fig. 8.3, and better robustness was confirmed by mechanical stability of the three contact points rather than improvement of chemical bond strength [124]. Interestingly, the observed electric conductance of diphenylacetylene anchored by **3Py** is about 140 times larger than that of a single pyridine (**1Py**) anchor unit, in which the tunneling channel is π orbital of N atom. In order to understand the distinct nonadditive contact effect of **1Py** and **3Py**, first-principles calculations are necessary. Two structures of the surface electrodes, (111) and (001), were adopted as computational model systems to perform NEGF-DFT. The resulting σ of the former **3Py** junction was $1.16\times10^{-6}G_0$, which is close to **1Py**. On the contrary, σ of **3Py** (001) electrodes was $2.27 \times 10^{-4}G_0$. The molecular orbital relating to the tunneling is given in Fig. 8.4, and the first-principles results predict formation of π contact at (001) electrode. In other words, the high conductance of the **3Py** anchor can be explained by formation of π contact. The presented example shows importance of "contact chemistry" to design the molecular device [125].

NEGF-DFT is used to calculate not only coherent (ballistic) current but also inelastic electric current by electron-vibron scatterings and is applied to assign IETS [126–134]; however, most of the calculations have been performed within the perturbation theory or LOE theory and applied to assign IETS. The LOE has more simplified expression than that of the rigorous lowest-order Born expansion [103] by

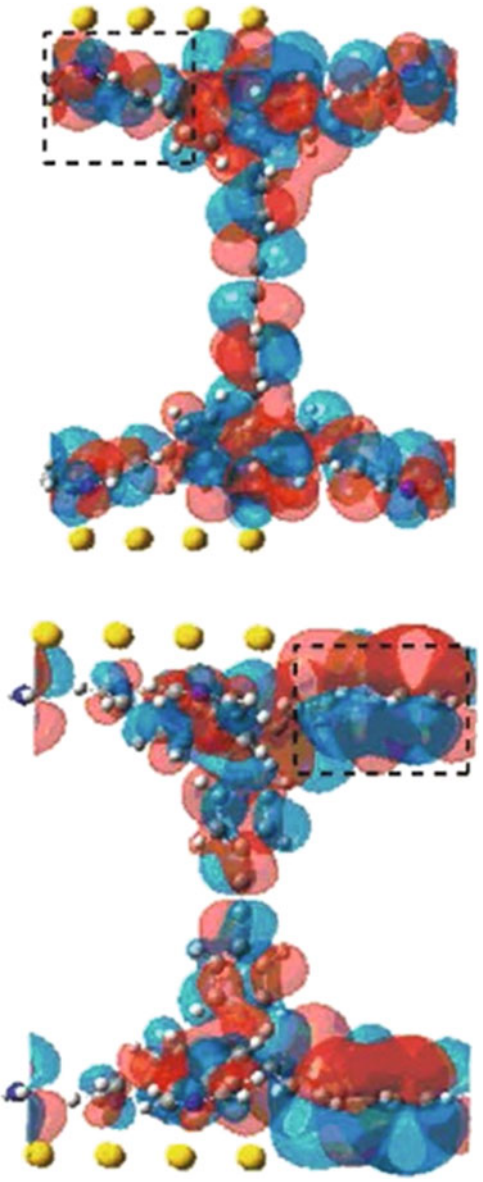

Fig. 8.4 The plot of wave function of conducting molecular orbital of 3Py junction for Au(111) (*left panel*) and Au(001) electrodes (*right panel*), respectively [124]

introducing approximations like energy averaging [47] and/or WBL [101, 102] and so on. In the standard LOE method implemented to the NEGF-DFT, vibron Green's function D is represented by normal mode coordinates, and the self-energy $\Pi_L^r + \Pi_R^r$ is parameterized to damping constant η_α. This approximation still includes the nonequilibrium term of vibron (vibron excitation) though it is not accurate enough to estimate local heating. LOE is a practical approach to combine first-principles

methods and applicable to simulate inelastic processes at low bias when the tunneling is off-resonant or resonance is not as narrow as the scale of Ω_α. Comparison of the IETS signals by experiments and NEGF-DFT calculations has been studied very actively. Typically, agreement of the shape and peak/dip positions is fairly well for alkane-dithiol chain systems and metal atomic wires. Comparing with these alkane chains, agreement is not sufficient quantitatively for aromatic molecular junctions (e.g., benzene-dithiol), in particular for asymmetric low-frequency modes. Since most of aromatic molecular backbones have high symmetry, IETS is very sensitive to conformation of the molecule, electrodes, and adsorbed structure. Small perturbation easily mixes different irreducible representation modes: thus, more precise measurement and careful computational modeling will be necessary to get quantitative agreement. However, for qualitative assignment of IETS signals and active vibrational modes, NEGF-DFT and LOE provide useful insight.

In Fig. 8.5, (a) the first-principles IETS of benzene-dithiol and (b) four Au atomic wires attached on the Au electrodes are presented. Temperature was fixed with 5.0 K. For simplicity, only three longitudinal modes were included for the Au wire, while all molecular internal modes were considered for the benzene-dithiol junction. Difference of IETS shape (dip/peak) is clearly presented. In both cases, some phonon damping parameters η_α were examined. Let us consider the two limited cases. One is $\eta_\alpha \to \infty$ (damped limit), which represents that the excitation energy is relaxed instantaneously to the electrodes and vibron is always in thermal equilibrium. The other is $\eta_\alpha \to 0$ (undamped limit), where thermal dissipation is assumed to be very slow. With decreasing η_α (i.e., from damped limit to undamped), offset grows in IETS signal. Observed offset is caused by bias dependence of the distribution function of each vibron, which is deviation from N_{BE}. Since the total number of the internal modes of benzene-dithiol is 36, most of the normal modes are IETS *inactive*. The symmetry rule and propensity of IETS have been discussed for several groups [135–139], but they are not as simple as the rule of IR and Raman spectroscopy [130, 140]: thus, first-principles calculation is highly desirable to analyze experimental IETS signal.

Simulation of IETS is also a useful tool to identify the mechanism of current-induced chemical reaction [141]. Very recently, Ohto et al. examined NEGF-DFT to understand molecular switching mechanism of melamine on Cu electrode by STM [142]. Using nudged elastic band method [143] and IETS calculation, they found that the reaction coordinate of the conformation switch agrees with the highly IETS active mode. By following calculations of current-induced adiabatic force and electric field effect [144, 145], they concluded that switching is dominated by direct vibrational heating of the promoting mode. Then the action spectra are calculated by performing current-induced reaction dynamics using first-principles data. They also found that the backward reaction is forbidden by less vibrational heating because of nearly zero IETS intensity of the relating mode. This is consistent with experimental observation [146].

In addition to NEGF-DFT calculations of observable properties like *IV*, extracting some first-principles data and parameterizing model Hamiltonian will be very useful to screening research of device material design and/or to attack challenging

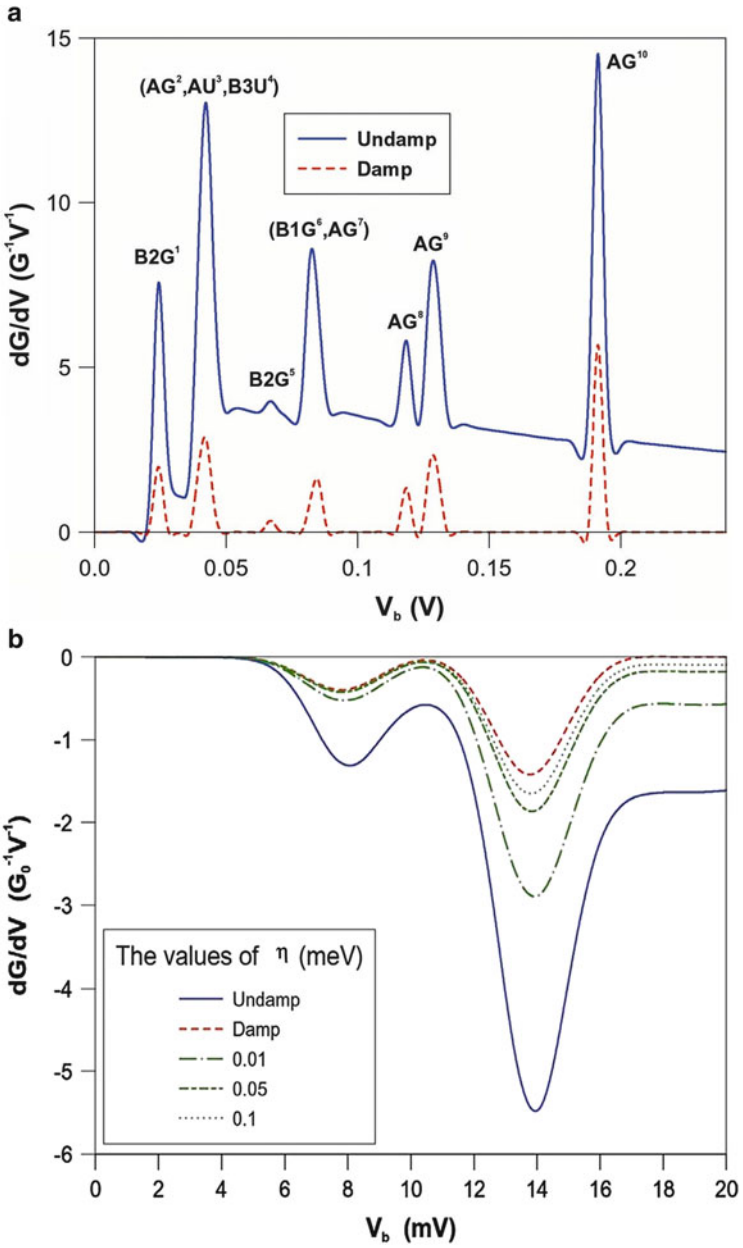

Fig. 8.5 Calculated IETS of benzene-dithiol (**a**) and four Au atomic chains (**b**). Only three longitudinal modes are included in the calculation of the Au chain. The label in the *upper panel* represents irreducible representation of the group of the assigned vibrational modes. The adopted damping factor of each plot is in the insets [48]

transport problems beyond DFT without huge computational demands. In the following, we describe a systematic theoretical method to extract characteristic quantities bridging traditional MO theory and NEGF approach. In order to analyze intrinsic molecular properties, MO theory is the most popular and powerful utility. The design of functional molecules by tuning energy and phase of the frontier MOs (highest occupied MO, HOMO, or lowest occupied MO, LUMO) by chemical modification or chemical substitution is one of (atomistic) chemical engineering, i.e., MO engineering [147]. MO engineering should be a key to create a desired device. However, hybridization of MOs and continuum states of the electrodes changes the electronic structure of "free" molecules and charge donation/back donation through the contact shift energy alignment relative to E_F. Furthermore, electronic interaction between molecular and metal electronic states governs both mechanical strength and conductance as illustrated in the tripodal anchoring system. Hence fusion of MO engineering and contact chemistry is desired.

One of the straightforward approaches is calculating transmission eigenchannel wave functions, and another is adopting an MO picture based on effective Hamiltonian formalism [148]. The former approach is given in Ref. [149]. The latter scheme consists of (i) defining Hamiltonian projected onto the focused molecular region (this projected Hamiltonian is often called molecular projected state Hamiltonian, MPSH) [150] and then (ii) renormalizing the remaining part by projection operator technique [13]. When the projection operators to focused molecular region, left outer region, and right outer region are denoted as P, QL, and Q_R, respectively, the effective Hamiltonian on the P space is

$$H_{PP}^{eff}(E) = H_{PP} + H_{PQ_L}G_{QQ}(E)H_{Q_LP} + H_{Q_RP}G_{QQ}(E)H_{PQ_R} \tag{8.20}$$

where X_{YY} represents YXY. The H_{PP} term is the MPSH. Q is equal to $QL + Q_R$ and $P + Q_L + Q_R = 1$ as the operator. The eigenstates of MPSH define MO basis $\{\varphi_\alpha\}$ and this is termed as projected MO (PMO). In contrast to MOs of a free molecule, the PMO has a complex energy term by the last two terms in Eq. 8.20:

$$\begin{aligned}\bar{\varepsilon}_\alpha =& < \varphi_\alpha \left| H_{PP} \right| \varphi_\alpha > + < \varphi_\alpha \left| \mathrm{Re}\left(H_{PQ_L}G_{QQ}H_{Q_LP} + H_{Q_RP}G_{QQ}H_{PQ_R} \right) \right| \varphi_\alpha > \\ &+ i < \varphi_\alpha \left| \mathrm{Im}\left(H_{PQ_L}G_{QQ}H_{Q_LP} \right) \right| \varphi_\alpha > + i < \varphi_\alpha \left| \mathrm{Im}\left(H_{PQ_R}G_{QQ}H_{Q_RP} \right) \right| \varphi_\alpha > \\ &= \varepsilon_\alpha(E) - i\gamma_L(E) - i\gamma_R(E)\end{aligned} \tag{8.21}$$

where the real values ε_α and $\gamma_{L/R}$ represent the PMO energy and electronic coupling strength with the left (right) electrode, respectively. The term ε_α consists of an energy shift by orbital hybridization of PMO and wave functions of electrodes. The complex orbital energy $\bar{\varepsilon}_\alpha$ depends on energy E. Only when one focuses on low bias voltage E may be fixed with E_F. The first-order contribution of φ_α to the

conductance is evaluated by the Breit-Wigner form as

$$\tau_\alpha = \frac{4\gamma_L\gamma_R}{(E_F - \varepsilon_\alpha)^2 + (\gamma_L + \gamma_R)^2}, \tag{8.22}$$

and one can identify the conducting MO by checking each τ_α. Note that all parameters can be calculated by NEGF-DFT directly and these parameters include the orbital phase and contact effect implicitly, i.e., straightforward extension of MO engineering unified with contact chemistry.

Using the effective Hamiltonian, site energy alignment for conduction is roughly estimated. To obtain site energies, further division of the P space to three subspaces and then diagonalization of each sub-block matrix of H_{PP} (not H_{PP}^{eff}) are performed. The resulting eigenvector relates localized molecular orbitals (MOs) on each site. Then (renormalized) site energy can be obtained as the matrix elements of $H_{PP}^{eff}(E_F)$ in the (new) localized MO basis on each group [13].

8.3 Rectification by a Single *pn* Molecule with Symmetric Anchors and Electrodes: Aviram-Ratner or Ellenbogen-Love Diode?

In the following sections, a unimolecular rectifier of a *pn* resembled diblock molecule [151–156] is discussed. The diode molecule proposed by AR (AR diode molecule) consists of π-Donor (πD) and π-Acceptor (πA) molecular groups separated by a σ spacer bond, and it has often been denoted as D-σ-A [10]. The πA (πD) part plays an analogous role as p-type (n-type) semiconductor of the bulk *pn* junction, and the forward direction of the AR diode is same with that of bulk *pn* diode. Based on AR's idea, many D-σ-A and several D-π-A structure molecules have been synthesized, and asymmetric IV characteristics have been observed in a high bias voltage regime (typically above 1.5 V) [157–160]. However, most of the proposed D-σ-A molecules consist of an asymmetric contact because D and A groups are usually completely different molecules. Hence, it is not clear that rectification is triggered by the intrinsic electronic structure of the separated D and A or by the asymmetric structure of the contact.

In the AR model, the energy alignment of HOMO of πD group and LUMO of πA relative to E_F is focused and effects of nonequilibrium electronic response of HOMO and/or LUMO to finite bias is omitted. On the contrary to AR, Ellenbogen and Love (EL) focused on the change of energy gap between MOs localized on πD and πA by applied bias direction [12]. The forward direction in the EL mechanism is *opposite* to that of the *pn* because the positive bias voltage of $\pi A \rightarrow \pi D$ direction is expected to lift up the HOMO level of πD while it may diminish the LUMO energy of πA. NEGF-DFT calculations have been examined to various D-σ-A rectification molecules and the results supported EL mechanism [15, 161].

On the side of *IV* measurement experiments, a key to make "molecular" rectification mechanism clear is (i) arranging symmetric electrodes and anchors in the junction and (ii) identifying forward direction with regulated orientation in single-molecule level. Only very recently, the precise measurement of the unimolecular rectifier satisfying (i) and (ii) is performed [154, 155]. Recently, several experimental groups have observed clear rectification behavior in a series of self-assembled monolayers (SAMs) made of *pn* resembled diblock molecules instead of a *D*-σ-*A* structure [151, 154–156]. The forward direction in these cases agrees with that of *pn* junctions. The latest study includes single molecular diode property found experimentally in a specific form of the diblock molecules, i.e., bipyrimidinyl-biphenyl molecule with the symmetric thiol anchors. *IV* characteristics of the bipyrimidinyl-biphenyl asymmetric molecule were compared with that of its symmetric counterpart, i.e., tetraphenyl molecule [155]. This leads to an experimental finding that the rectification of the asymmetric molecule starts from very low voltage. These experimental findings conflict with EL mechanism: thus, the question is that if rectification is realized by classical AR or alternative mechanism relating an intrinsic *pn* feature *built in* the diblock molecule.

The NEGF-DFT was applied to the asymmetric and symmetric molecules, then, clear asymmetry was found in the *IV* curve of the single asymmetric. The rectification ration, $\eta(V) = I_{\text{forward}}/I_{\text{backword}}$, is 1.34 and 1.58 for $V = 0.5$ and 1.0 volt, respectively. In particular, the rectification ration of first-principles and experimental results agrees well in the low-bias region $V \leq 0.5$ volt. This result shows that qualitative parameters such as $\eta(V)$ by NEGF-DFT are sufficiently reliable though NEGF-DFT by local density approximation (LDA) or generalized gradient approximation (GGA) XC functions often overestimate the absolute value of conductance and electric current. The agreement between the theoretical and the experimental results in this region is excellent, while the difference grows rapidly as we increase bias voltage above 0.6 V.

The forward direction of rectification obtained by the calculation agrees with the experiments, i.e., it behaves in the same way as the standard *pn* junction. To understand the mechanism of the *pn* forward direction, analysis of PMOs for electric transport channels and their bias dependence are useful. According to Eq. 8.22, both ε_α and the product of $\gamma_{\alpha L}$ and $\gamma_{\alpha R}$ (or square root of $\gamma_L\gamma_R$) are important in characterizing "conducting" molecular orbitals. For example, let us consider an extreme case where $1 \ll \gamma_L$ and $\gamma_R = 0$. The electric current through the molecule is negligibly small in this limit even when $\varepsilon_\alpha \approx E_F$ (i.e., resonant tunneling) and $\gamma_L + \gamma_R$ is large. The parameters ε_α and the square root of the molecule-electrode coupling product $\sqrt{\gamma_{\alpha L}\gamma_{\alpha R}}$ were used to identify conducting PMOs. E_F is set to zero below.

In Table 8.1, values of $\left(\varepsilon_\alpha, \sqrt{\gamma_{\alpha L}\gamma_{\alpha R}}\right)$ for HOMO-1, HOMO, and LUMO were listed. Here, note that the terminologies of HOMO/LUMO for the PMOs are defined by a relative energy level of ε_α to E_F for each bias case as usual. They were obtained from our first-principles analyses at $V = \pm 0.4$ and $V = \pm 0.8$ volt, respectively. The target molecule projected out by the projection operator P then is the dithiolated diblock molecule. In the case of the single symmetric molecular

Table 8.1 PMO energies and the square root product of the molecule-electrode couplings for tetraphenyl (symmetric molecular junction) and bipyrimidinyl-biphenyl (asymmetric molecular junction). Results of HOMO-1, HOMO, and LUMO are listed where E_F is set to 0. The bold italic parts indicate the dominant PMOs for tunneling. The units of bias and energy (coupling strength) are volt and eV, respectively (Data taken from Ref. [13])

Tetraphenyl						
Bias	E_{H-1}	$\sqrt{\gamma_L\gamma_R}$	E_H	$\sqrt{\gamma_L\gamma_R}$	E_L	$\sqrt{\gamma_L\gamma_R}$
−0.8	−1.90	0.433	***−0.97***	***0.162***	2.01	0.090
−0.4	−1.72	0.331	***−1.05***	***0.142***	2.01	0.062
0.4	−1.84	0.358	***−1.02***	***0.143***	2.08	0.071
0.8	−1.80	0.489	***−0.99***	***0.166***	1.95	0.113
Bipyrimidinyl-biphenyl						
Bias	E_{H-1}	$\sqrt{\gamma_L\gamma_R}$	E_H	$\sqrt{\gamma_L\gamma_R}$	E_L	$\sqrt{\gamma_L\gamma_R}$
−0.8	***−1.41***	***0.285***	−1.00	0.011	1.63	0.071
−0.4	***−1.31***	***0.152***	−1.21	0.044	1.60	0.042
0.4	−1.42	0.018	***−1.18***	***0.106***	1.44	0.038
0.8	−1.50	0.048	***−1.09***	***0.144***	1.35	0.065

junction system, the most dominant PMO for electric current is the HOMO, and $\sqrt{\gamma_{\alpha L}\gamma_{\alpha R}}$ is symmetric with respect to the sign change of bias voltage. On the contrary, $\sqrt{\gamma_{\alpha L}\gamma_{\alpha R}}$ of the single asymmetric molecular junction system depends much more on the voltage sign. At positive bias, drastic asymmetry of electronic coupling strength to electrodes was obtained, i.e., $\sqrt{\gamma_{\alpha L}\gamma_{\alpha R}} << 1$ for HOMO-1, while it was observed at negative bias voltage for HOMO, i.e., the conducting MO is switched from HOMO to HOMO-1. This switch is an *intrinsic* property as a result of finite bias response of phase and amplitude of MOs, and the complex MO energies should be derived by the effective Hamiltonian. The rectification is realized by this switching because electric current through HOMO-1 should be smaller than that through HOMO because of a larger gap between HOMO-1 and E_F.

Similar MPSH analysis has been successfully applied to several other molecular diodes [15, 162]. For an example, Stadler et al. discussed a theoretical view of unimolecular rectification by PMO energy curves of a function of bias voltage V, where they determined PMO energies by the peak position of $\tau(E)$ [14, 163]. The spaghetti-like PMO energy curves are somewhat similar with Born-Oppenheimer (BO) potential energy curves of a molecular system; however, the latter is defined as a function of reaction coordinate. When one adopts a "diabatic" representation, which can be defined as the states "enforcing smoothness of some physical property or electronic structure" [164, 165], the diabatic MOs can be defined by enforcing smoothness of the value of $\gamma_L\gamma_R$ as a function of V. Clear rectification is then a result of avoided crossing by diabatic coupling between conducting and non-conducting diabatic MOs.

In order to get a more intuitive picture, the site energy alignment of the above asymmetric molecule is illustrative. Argument of similarity and difference with AR mechanism or EL mechanism is possible by site (complex) energy alignment as

well. The diblock molecule is represented by four sites, i.e., two phenyl groups and two pyrimidinyl groups for the asymmetric molecule and four phenyl groups for the symmetric molecule, respectively. The most left and right sites include anchor atoms. The site energy alignment of the single symmetric molecular junction changes symmetrically by varying the polarity of V. The site energy of the right edge phenyl group decreases by 2.01 eV when the V is increased from −0.8 to 0.8 V, although the change of the site energy of the two middle groups is much smaller (0.22 eV) than that of the edge groups. This behavior is consistent with the fact that the phenyl molecule is electron accepting, i.e., it is n type (πA). It is also reasonable because we expect that the molecule-electrode interaction effect is mostly limited to the edge molecular groups. On the other hand, the change at the edge pyrimidinyl site (0.63 eV) is much smaller than that of the edge phenyl site. The change of site energy alignment induced by bias voltage is analogous to what is expected in the reduction of built-in potential or smoothed slope of band bending by forward bias in the bulk pn junction. The intended direction of charge migration is given by πD (pyrimidinyl) $\rightarrow$ πA (phenyl) in the EL mechanism, while πD πA favored bias-induced change of electronic coupling strength of πA-LUMO which is much smaller than πA-HOMO (<1.0 %) in the present pn resembled molecule. Thus, the EL mechanism is not likely [13].

After demonstrating the asymmetric IV characteristics in a low bias voltage regime, the IETS was measured to explore effects of the diode property to inelastic current and heating [155]. According to Eq. 8.16, enhanced asymmetry is expected in the inelastic current of the diode molecule. In Fig. 8.6, the measured and calculated IETS of the bipyrimidinyl-biphenyl is plotted. Note that both plots are obtained by subtracting the derivative of elastic current, and $-\frac{d^2I}{dV^2}$ is plotted when bias is negative. As same with IV characteristics, symmetric tetraphenyl was also

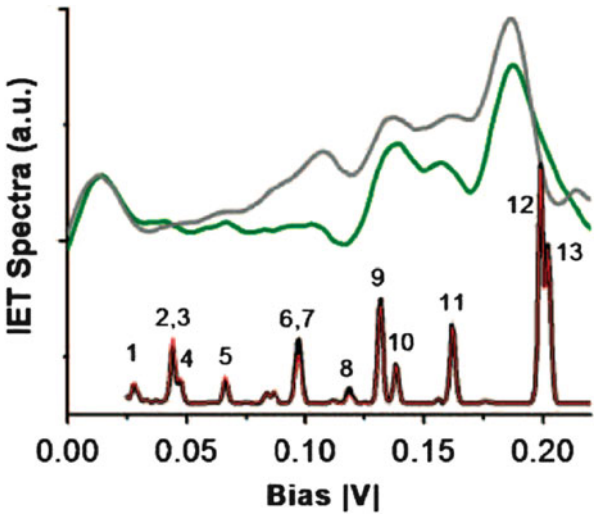

Fig. 8.6 Subtracted IETS in low-bias regime. The *thick green curve* is for positive bias and the *thin gray curve* is the negative bias region rotated 180°. The *black* and *red curves* are the calculated IETS in positive and negative bias, respectively [155]

examined for comparison. Although slight asymmetries in the peak intensity may be due to either effect from the conformation of the junction or from asymmetry of electron-vibron coupling, they do not show consistent asymmetric intensity across the molecular junction. Asymmetry is much smaller than that expected by Eq. 8.14 and it is almost symmetric for the fingerprint modes. Theoretical results by NEGF-DFT support nearly symmetric intensity. Recall that symmetric electronic coupling strength (in this case, $\gamma_{\alpha L} \approx \gamma_{\alpha R}$) is assumed when Eq. 8.14 is derived. The *bias-dependent* asymmetry of electronic coupling strength as well as the MO energy level works to suppress asymmetry of IETS intensity in the present system.

8.4 Summary

In this chapter, modern views of molecular electric transport were presented based on concerto of theoretical models and first-principles calculations. Some illustrative examples of applications to electric and energy-harvesting devices were presented to clarify our views. Actually, study of molecular electronics has a long history, and there are many interesting experimental findings relating to functional devices; however, there are several problems to creating a practical device and circuit, yet. The theory of molecular junction is just a border of the transport theory in solid or mesoscopic physics and electron transfer theory in chemistry. The unified views are very useful to make a bridge of theoretical approaches in physics and chemistry communities.

The basic theory of length and temperature dependence of molecular conductance or electron transfer rate is sometimes considered to be a textbook example; however, there are rooms to deepen the theory and to refine the model in order to explain recent experimental findings such as even/odd oscillation of conductance, crossover of length and temperature dependence, and so on. The last problem relates to a fundamental but difficult issue: how to handle electron-phonon or electron-vibron scatterings in a nano-contact. Effort of theoretical and computational modeling and application to practical systems will give a new insight to local heating and Joule heating in broader nanoelectronics.

A single molecular rectifier by adopting a *pn* diblock molecule rather than a classical *D*-σ-*A* structure was analyzed to identify really "intrinsic" rectification of the molecule where symmetric anchors, controlled molecular orientation to the electrodes, and clear identification of forward/backward bias polarity to the molecular orientation are required. NEGF-DFT and effective MPSH analysis merged MO and transport theories. A view of MO engineering and contact chemistry provides modern classification of a molecular rectifier. This is one of the successful examples to prove the usefulness and power of first-principles transport calculation. Of course, the present status of first-principles transport calculation is not sufficient because of lack of electron correlation. With developing computational algorithm of "beyond NEGF-DFT," theoretical development is required for nonequilibrium quantum transport. A molecular rectifier is a good target to tackle this nonequilibrium

electron correlation problem. Potentiality of molecular junctions and designing suitable materials to high-efficiency energy-harvesting devices is more challenging. Theoretical aspects shown in this article are applicable to more general devices like metal oxide bulk heterojunctions, Si materials, and so on, where a sub-10 n scale is now in the scope. It seems evident that understanding and controlling the quantum nature of transport have large capability to tailor-made functional device.

Acknowledgments The author would like to thank for fruitful discussion with Dr. Yoshihiro Asai.

References

1. van Ruitenbeek JM, Alvarez A, Pineyro I, Grahmann C, Joyez P, Devoret MH, Esteve D, Urbina C (1996) Rev Sci Instrum 67:108–111
2. Waitz R, Schecker O, Scheer E (2008) Rev Sci Instrum 79. 093901-1-5
3. Tsutsui M, Shoji K, Taniguchi M, Kawai T (2008) Nano Lett 8:345–349
4. Rubio G, Agrait N, Vieira S (1996) Phys Rev Lett 76:2302–2305
5. Beebe JM, Kim B, Frisbie CD, Kushmerick JG (2008) ACS Nano 2:827–832
6. Chen J, Reed MA, Rawlett AM, Tour JM (1999) Science 286:1550–1552
7. Markussen T, Chen JZ, Thygesen KS (2011) Phys Rev B 83. 155407-1-6
8. Reed MA, Zhou C, Deshpande MR, Muller CJ, Burgin TP, Jones L, Tour JM (1998) Mol Electron: Sci Technol 852:133–144
9. Xu BQ, Tao NJJ (2003) Science 301:1221–1223
10. Aviram A, Ratner MA (1974) Chem Phys Lett 29:277–283
11. Sze SM, Ng KK (2007) Physics of semiconductor devices. Wiley, New York
12. Ellenbogen JC, Love JC (2000) Proc IEEE 88:386–426
13. Nakamura H, Asai Y, Hihath J, Bruot C, Tao N (2011) J Phys Chem C 115:19931–19938
14. Stadler R, Geskin V, Cornil J (2008) J Phys Condens Matter 20:374105
15. Stokbro K, Taylor J, Brandbyge M (2003) J Am Chem Soc 125:3674–3675
16. Gao J, Yu G, Heeger AJ (1998) Adv Mater 10:692–695
17. Halls JJM, Pichler K, Friend RH, Moratti SC (1996) Appl Phys Lett 68:3120–3122
18. Steim R, Kogler FR, Brabec CJ (2010) J Mater Chem 20:2499–2512
19. Yu G, Gao J, Hummelen JC, Wudl F, Heeger AJ (1995) Science 270:1789–1791
20. Bubnova O, Crispin X (2012) Energ Environ Sci 5:9345–9362
21. Bubnova O, Khan ZU, Malti A, Braun S, Fahlman M, Berggren M, Crispin X (2011) Nat Mater 10:429–433
22. Finch C, García-Suárez V, Lambert C (2009) Phys Rev B 79:033405
23. Liu Y-S, Chen Y-R, Chen Y-C (2009) ACS Nano 3:3497–3504
24. Malen JA, Yee SK, Majumdar A, Segalman RA (2010) Chem Phys Lett 491:109–122
25. Murphy P, Mukerjee S, Moore J (2008) Phys Rev B 78:161406
26. Reddy P, Jang SY, Segalman RA, Majumdar A (2007) Science 315:1568–1571
27. Bahrami A, Dogan F, Japrung D, Albrecht T (2012) Biochem Soc Trans 40:624–628
28. Tsutsui M, Rahong S, Iizumi Y, Okazaki T, Taniguchi M, Kawai T (2011) Sci Rep UK 1:1–6
29. Zwolak M, Di Ventra M (2005) Nano Lett 5:421–424
30. Browne WR, Feringa BL (2006) Nat Nanotechnol 1:25–35
31. Chen J, Wang W, Klemic J, Reed MA, Axelrod BW, Kaschak DM, Rawlett AM, Price DW, Dirk SM, Tour JM, Grubisha DS, Bennett DW (2002) Ann N Y Acad Sci 960:69–99
32. Eigler DM, Lutz CP, Rudge WE (1991) Nature 352:600–603
33. Huang T, Zhao J, Peng M, Popov AA, Yang SF, Dunsch L, Petek H (2011) Nano Lett 11:5327–5332

34. Simonian N, Likharev KK, Mayr A (2013) J Appl Phys 113. 044504-1-14
35. Sahu S, Pal AJ (2008) Org Electron 9:873–877
36. Bergfield JP, Solomon GC, Stafford CA, Ratner MA (2011) Nano Lett 11:2759–2764
37. Ke SH, Yang WT, Baranger HU (2008) Nano Lett 8:3257–3261
38. Nakamura H, Yamashita K (2008) Nano Lett 8:6–12
39. Solomon GC, Andrews DQ, Van Duyne RP, Ratner MA (2008) J Am Chem Soc 130:7788
40. Datta S (1995) Electronic transport in mesoscopic systems. Cambridge University Press, Cambridge
41. Kadanoff LP, Baym G (1962) Quantum statistical mechanics. Benjamin, New York
42. Keldysh LV (1965) Sov Phys JETP USSR 20:1018
43. Wingreen NS, Jauho AP, Meir Y (1993) Phys Rev B 48:8487–8490
44. Brandbyge M, Mozos JL, Ordejon P, Taylor J, Stokbro K (2002) Phys Rev B 65:165401
45. Kong LT, Denniston C, Muser MH (2011) Comput Phys Commun 182:540–541
46. Luisier M, Schenk A (2008) J Comput Theor Nanosci 5:1031–1045
47. Nakamura H, Yamashita K (2006) J Chem Phys 125:194106
48. Nakamura H, Yamashita K, Rocha AR, Sanvito S (2008) Phys Rev B 78:235420
49. Rungger I, Sanvito S (2008) Phys Rev B 78:035407
50. Sanvito S, Rocha AR (2006) J Comput Theor Nanosci 3:624–642
51. Stokbro K, Taylor J, Brandbyge M, Ordejon P (2003) Mol Electron III 1006:212–226
52. Toher C, Sanvito S (2007) Phys Rev Lett 99:056801
53. Xue YQ, Datta S, Ratner MA (2002) Chem Phys 281:151–170
54. Taylor J, Guo H, Wang J (2001) Phys Rev B 6324:245407
55. May V, Kühn O (2000) Charge and energy transfer dynamics in molecular systems. Wiley-VHC, Berlin
56. Nitzan A (2006) Chemical dynamics in condensed phases. Oxford University Press, Oxford
57. Luo L, Frisbie CD (2010) J Am Chem Soc 132:8854
58. Luo LA, Choi SH, Frisbie CD (2011) Chem Mater 23:631–645
59. Joachim C, Ratner MA (2005) Proc Natl Acad Sci U S A 102:8801–8808
60. Engelkes VB, Beebe JM, Frisbie CD (2004) J Am Chem Soc 126:14287–14296
61. Selzer Y, Cabassi MA, Mayer TS, Allara DL (2004) Nanotechnology 15:S483–S488
62. Selzer Y, Cabassi MA, Mayer TS, Allara DL (2004) J Am Chem Soc 126:4052–4053
63. Mujica V, Nitzan A, Mao Y, Davis W, Kemp M, Roitberg A, Ratner MA (1999) Electron transfer in molecules and molecular wires: geometry dependence, coherent transfer, and control. In: J Jortner, M Bixon (eds) Electron transfer, vol 107. Wiley, pp 403–430
64. Choi SH, Kim B, Frisbie CD (2008) Science 320:1482–1486
65. He J, Chen F, Li J, Sankey OF, Terazono Y, Herrero C, Gust D, Moore TA, Moore AL, Lindsay SM (2005) J Am Chem Soc 127:1384–1385
66. Salomon A, Cahen D, Lindsay S, Tomfohr J, Engelkes VB, Frisbie CD (2003) Adv Mater 15:1881–1890
67. Sikes HD, Smalley JF, Dudek SP, Cook AR, Newton MD, Chidsey CED, Feldberg SW (2001) Science 291:1519–1523
68. Choi SH, Risko C, Delgado MCR, Kim B, Bredas JL, Frisbie CD (2010) J Am Chem Soc 132:4358–4368
69. Yan HJ, Bergren AJ, McCreery R, Della Rocca ML, Martin P, Lafarge P, Lacroix JC (2013) Proc Natl Acad Sci U S A 110:5326–5330
70. Lloveras V, Vidal-Gancedo J, Figueira-Duarte TM, Nierengarten JF, Novoa JJ, Mota F, Ventosa N, Rovira C, Veciana J (2011) J Am Chem Soc 133:5818–5833
71. Smit RHM, Untiedt C, Rubio-Bollinger G, Segers RC, van Ruitenbeek JM (2003) Phys Rev Lett 91. 076805-1-4
72. Smit RHM, Untiedt C, van Ruitenbeek JM (2004) Nanotechnology 15:S472–S478
73. Asai Y, Fukuyama H (2005) Phys Rev B 72:085431
74. Yeganeh S, Ratner MA, Mujica V (2007) J Chem Phys 126:161103
75. Lang IG, Firsov YA (1963) Sov Phys JETP USSR 16:1301–1312

76. Mahan G (1990) Many-particle physics. Plenum, New York
77. Marcus RA, Sutin N (1985) Biochim Biophys Acta 811:265–322
78. Coropceanu V, Cornil J, da Silva DA, Olivier Y, Silbey R, Bredas JL (2007) Chem Rev 107:926–952
79. Yoo KH, Ha DH, Lee JO, Park JW, Kim J, Kim JJ, Lee HY, Kawai T, Choi HY (2001) Phys Rev Lett 87:198102
80. Sepunaru L, Friedman N, Pecht I, Sheves M, Cahen D (2012) J Am Chem Soc 134:4169–4176
81. Lee SK, Yamada R, Tanaka S, Chang GS, Asai Y, Tada H (2012) ACS Nano 6:5078–5082
82. Asai Y (2008) Phys Rev B 78:045434
83. Gregory S (1990) Phys Rev Lett 64:689–692
84. Hahn JR, Lee HJ, Ho W (2000) Phys Rev Lett 85:1914–1917
85. Stipe BC, Rezaei HA, Ho W (1999) Phys Rev Lett 82:1724–1727
86. Stipe BC, Rezaei MA, Ho W (1998) Science 280:1732–1735
87. Ho W (2002) J Chem Phys 117:11033–11061
88. Klein J, Leger A, Belin M, Defourne D, Sangster MJ (1973) Phys Rev B 7:2336–2348
89. Jaklevic RC, Lambe J (1966) Phys Rev Lett 17:1139
90. Lambe J, Jaklevic RC (1968) Phys Rev 165:821
91. Reed MA (2008) Mater Today 11:46–50
92. Galperin M, Ratner MA, Nitzan A (2004) J Chem Phys 121:11965–11979
93. Okabayashi N, Konda Y, Komeda T (2008) Phys Rev Lett 100:226604
94. Hihath J, Arroyo CR, Rubio-Bollinger G, Tao NJ, Agrait N (2008) Nano Lett 8:1673–1678
95. Hihath J, Bruot C, Tao NJ (2010) ACS Nano 4:3823–3830
96. Wang WY, Lee T, Kretzschmar I, Reed MA (2004) Nano Lett 4:643–646
97. Taniguchi M, Tsutsui M, Yokota K, Kawai T (2009) Nanotechnology 20:434008
98. Tsutsui M, Taniguchi M, Shoji K, Yokota K, Kawai T (2009) Nanoscale 1:164–170
99. Agrait N, Untiedt C, Rubio-Bollinger G, Vieira S (2002) Chem Phys 281:231–234
100. Agrait N, Untiedt C, Rubio-Bollinger G, Vieira S (2002) Phys Rev Lett 88:216803
101. Frederiksen T, Paulsson M, Brandbyge M, Jauho AP (2007) Phys Rev B 75:205413
102. Paulsson M, Frederiksen T, Brandbyge M (2005) Phys Rev B 72:033408
103. Viljas JK, Cuevas JC, Pauly F, Hafner M (2005) Phys Rev B 72:245415
104. Galperin M, Ratner MA, Nitzan A (2007) J Phys Condens Matter 19:103201
105. Shimazaki T, Asai Y (2008) Phys Rev B 77:115428
106. Andrews DQ, Solomon GC, Goldsmith RH, Hansen T, Wasielewski MR, Van Duyne RP, Ratner MA (2008) J Phys Chem C 112:16991–16998
107. Solomon GC, Andrews DQ, Goldsmith RH, Hansen T, Wasielewski MR, Van Duyne RP, Ratner MA (2008) J Am Chem Soc 130:17301–17308
108. Arroyo CR, Tarkuc S, Frisenda R, Seldenthuis JS, Woerde CHM, Eelkema R, Grozema FC, van der Zant HSJ (2013) Angew Chem Int Edit 52:3152–3155
109. Pecchia A, Penazzi G, Salvucci L, Di Carlo A (2008) New J Phys 10:065022
110. Rocha AR, Garcia-Suarez VM, Bailey S, Lambert C, Ferrer J, Sanvito S (2006) Phys Rev B 73:085414
111. Sanvito S, Lambert CJ, Jefferson JH, Bratkovsky AM (1999) Phys Rev B 59:11936–11948
112. Thygesen KS, Jacobsen KW (2005) Chem Phys 319:111–125
113. Jauho AP, Wingreen NS, Meir Y (1994) Phys Rev B 50:5528–5544
114. Galperin M, Nitzan A (2003) Mol Electron III 1006:48–67
115. Rocha AR, Garcia-Suarez VM, Bailey SW, Lambert CJ, Ferrer J, Sanvito S (2005) Nat Mater 4:335–339
116. Kurth S, Stefanucci G, Almbladh CO, Rubio A, Gross EKU (2005) Phys Rev B 72:035308
117. Kurth S, Stefanucci G, Khosravi E, Verdozzi C, Gross EKU (2010) Phys Rev Lett 104:236801
118. Stefanucci G, Kurth S, Rubio A, Gross EKU (2008) Phys Rev B 77:075339
119. Uimonen AM, Khosravi E, Stan A, Stefanucci G, Kurth S, van Leeuwen R, Gross EKU (2011) Phys Rev B 84:115103
120. Evers F, Schmitteckert P (2011) Phys Chem Chem Phys 13:14417–14420

121. Koentopp M, Burke K, Evers F (2006) Phys Rev B 73:121403
122. Strange M, Rostgaard C, Hakkinen H, Tygesen KS (2011) Phys Rev B 83:115108–1–115108–12
123. Thygesen KS, Rubio A (2008) Phys Rev B 77:115333
124. Ie Y, Hirose T, Nakamura H, Kiguchi M, Takagi N, Kawai M, Aso Y (2011) J Am Chem Soc 133:3014–3022
125. Chen F, Li XL, Hihath J, Huang ZF, Tao NJ (2006) J Am Chem Soc 128:15874–15881
126. Fu QA, Luo Y, Yang JL, Hou JG (2010) Phys Chem Chem Phys 12:12012–12023
127. Jiang J, Gao B, Hu ZP, Lu W, Wu ZY, Yang JL, Luo Y (2010) Appl Phys Lett 96:253110
128. Lin LL, Wang CK, Luo Y (2011) ACS Nano 5:2257–2263
129. Frederiksen T, Lorente N, Paulsson M, Brandbyge M (2007) Phys Rev B 75:235441
130. Nakamura H (2010) J Phys Chem C 114:12280–12289
131. Okabayashi N, Paulsson M, Ueba H, Konda Y, Komeda T (2010) Phys Rev Lett 104:077801
132. Long DP, Troisi A (2007) J Am Chem Soc 129:15303–15310
133. Troisi A, Ratner MA, Nitzan A (2003) J Chem Phys 118:6072–6082
134. Solomon GC, Gagliardi A, Pecchia A, Frauenheim T, Di Carlo A, Reimers JR, Hush NS (2006) J Chem Phys 124:094704
135. Gagliardi A, Solomon GC, Pecchia A, Frauenheim T, Di Carlo A, Hush NS, Reimers JR (2007) Phys Rev B 75:17
136. Paulsson M, Frederiksen T, Ueba H, Lorente N, Brandbyge M (2008) Phys Rev Lett 100:226604
137. Troisi A, Beebe JM, Picraux LB, van Zee RD, Stewart DR, Ratner MA, Kushmerick JG (2007) Proc Natl Acad Sci U S A 104:14255–14259
138. Troisi A, Ratner MA (2006) J Chem Phys 125. 214709-1-11
139. Troisi A, Ratner MA (2007) Phys Chem Chem Phys 9:2421–2427
140. Beebe JM, Moore HJ, Lee TR, Kushmerick JG (2007) Nano Lett 7:1364–1368
141. Cao H, Jiang J, Ma J, Luo Y (2008) J Phys Chem C 112:11018–11022
142. Ohto T, Rungger I, Yamashita K, Nakamura H, Sanvito S (2013) Phys Rev B 87. 205439-1-7
143. Henkelman G, Uberuaga BP, Jonsson H (2000) J Chem Phys 113:9901–9904
144. Todorov TN, Hoekstra J, Sutton AP (2000) Philos Mag B 80:421–455
145. Zhang RX, Rungger I, Sanvito S, Hou SM (2011) Phys Rev B 84. 085455-1-12
146. Pan SA, Fu Q, Huang T, Zhao AD, Wang B, Luo Y, Yang JL, Hou JG (2009) Proc Natl Acad Sci U S A 106:15259–15263
147. Fukui K (1982) Science 218:747–754
148. Feshbach H (1991) Theoretical nuclear physics: nuclear reactions. Weiley-Interscience, New York
149. Paulsson M, Brandbyge M (2007) Phys Rev B 76:201101
150. Stokbro K, Taylor J, Brandbyge M, Mozos JL, Ordejon P (2003) Comput Mater Sci 27:151–160
151. Ng MK, Lee DC, Yu LP (2002) J Am Chem Soc 124:11862–11863
152. Ng MK, Yu LP (2002) Angew Chem Int Edit 41:3598–3601
153. Oleynik II, Kozhushner MA, Posvyanskii VS, Yu L (2006) Phys Rev Lett 96:096803
154. Diez-Perez I, Hihath J, Lee Y, Yu LP, Adamska L (2009) Nat Chem 1:635–641
155. Hihath J, Bruot C, Nakamura H, Asai Y, Diez-Perez I, Lee Y, Yu LP, Tao NJ (2011) ACS Nano 5:8331–8339
156. Morales GM, Jiang P, Yuan SW, Lee YG, Sanchez A, You W, Yu LP (2005) J Am Chem Soc 127:10456–10457
157. Metzger RM (2009) Synth Met 159:2277–2281
158. Honciuc A, Metzger RM, Gong AJ, Spangler CW (2007) J Am Chem Soc 129:8310–8319
159. Jaiswal A, Rajagopal D, Lakshmikantham MV, Cava MP, Metzger RM (2007) Phys Chem Chem Phys 9:4007–4017
160. Ashwell GJ, Mohib A, Miller JR (2005) J Mater Chem 15:1160–1166

161. Pan JB, Zhang ZH, Deng XQ, Qiu M, Guo C (2011) Appl Phys Lett 98:013503
162. Ford MJ, Hoft RC, McDonagh AM, Cortie MB (2008) J Phys Condens Matter 20:374106
163. Stadler R, Geskin V, Cornil J (2008) Adv Funct Mater 18:1119–1130
164. Atchity GJ, Ruedenberg K (1997) Theor Chem Acc 97:47–58
165. Nakamura H, Truhlar DG (2001) J Chem Phys 115:10353–10372